A Simple Current Control of Permanent Magnet Synchronous Machines for Railway Traction Operating in Six-Steps

Xiaochun Fang [1], Zhongbei Tian [2*], Zhongping Yang [1], Fei Lin [1], Pietro Tricoli [3]

[1]The School of Electrical Engineering, Beijing Jiaotong University, Beijing, China
[2] Department of Electrical Engineering and Electronics, University of Liverpool, Liverpool, UK
[3] Department of Electronic, Electrical and Systems Engineering, University of Birmingham, Birmingham, UK
[*]zhongbei.tian@liverpool.ac.uk

Abstract: Due to the voltage limitation of the inverter DC-link of railway traction systems, six-step operations are widely used in the high-speed region to improve the voltage utilization and increase the maximum fundamental frequency. In fact, the magnitude of the output voltage fundamental harmonic reaches the maximum for six-step operations, while only the phase angle can be adjusted. This limitation makes it challenging to control the instantaneous current of permanent magnet synchronous motors (PMSM). This paper proposes a single *d*-axis current regulator flux-weakening control scheme to improve the current control over six-step operations of PMSM without changing the inverter output voltage modulation ratio by controlling only one degree of freedom. The voltage in six-step operations is generated by a synchronous space vector pulse width modulation (SVPWM) based on basic bus clamping strategy (BBCS) with an effective limitation of the switching frequency in the full-speed region. A simplified model of the current regulator is developed for the analysis and design of the controller parameters. This paper presents clear rules for entering and quitting six-step operations effectively to achieve a smooth transition between double current regulators and the single current regulator control. The numerical results are verified by experimental measurements on a 7.5 kW PMSM drive.

1. Introduction

Permanent Magnet Synchronous Motors (PMSM) achieve higher efficiency, higher power density, and lower maintenance cost than induction motors for a large number of applications [1-3]. Due to the outstanding performance, PMSMs have been widely used as railway traction motors. Due to the voltage limitation of the inverter DC-link, PMSMs require flux-weakening control to extend the operating speed beyond the base speed. Conventional PMSM flux-weakening algorithms are based on flux-oriented control. There are two current regulators, which are used to control the *d*-axis current and *q*-axis current, respectively. Double current regulators control can be obtained from the motor mathematical model [4, 5], lookup tables [6, 7], gradient descent of voltage limit [8], voltage feedback current control schemes [9, 10], etc.

In railway traction drive systems, the inverter generally enters six-step operations to utilize DC-link voltage when the motor is in the flux-weakening region. Compared with the linear region of the space vector pulse width modulation (SVPWM), the inverter output fundamental voltage amplitude is improved by 10.26% in six-step operations with consequent improvement of the output torque and working area. Six-step operations also reduce the switching frequency and, hence, inverter power loss.

Two basic problems need to be addressed to obtain satisfactory six-step operations of PMSMs. First, a suitable vector controller is required to achieve instantaneous motor control, as in six-step operations the phase angle of the inverter voltage is the only degree of freedom. The above mentioned conventional double current regulators control is difficult to work in six-step operations. Second, the maximum switching frequency of traction inverters is commonly below 1000 Hz. Thus, a proper synchronous PWM algorithm is required to limit low-order harmonics, reduce current distortion and ensure a smooth transition to and from six-step operations.

There are mainly two types of six-step control schemes for PMSMs in the technical literature. The first is the improved voltage feedback current control scheme [11-13]. This series of research is continuously improved for the realization of current closed-loop control in six-step operations. Finally, the study in [13] realizes the instantaneous current control in six-step operation by enhancing the coupling between *d*-axis and *q*-axis current regulators. As a double current regulators control scheme, this method is too complicated to interpret and implement. The second is the voltage phase angle control [14-16]. This scheme is a special and easily achieved flux-weakening control scheme for high power PMSM in six-step operations. The voltage phase angle is adjusted to follow the torque instruction. However, the dynamic response is slow as there is no current regulator. In [16], the torque regulator control parameters are adjusted using the PMSM model and the system dynamic performance is improved. However, the performance of this method depends on the accuracy of the knowledge of the machine parameters.

In addition, there are some other papers studying six-step operations of PMSM. A simple feedforward control scheme is proposed in [17]. However, as an open-loop method, the feedforward control has a slow dynamic response and high parameter dependence. In [18], the angle between the voltage vector and the *q*-axis is regulated by *q*-axis component of the current, and, then, PMSM six-step operations are achieved with a variable time step six-step modulation. The variable time step modulation is conflicting with traditional fixed-step PWM methods of traction inverters.

The performance of a control with double current regulators deteriorates when the voltage amplitude is limited because of the need to maintain the decoupling of the *d*-*q* axis currents. In response to this, a single current regulator control

is proposed in [19-21]. This method regulates the *d*-axis current to obtain the *d*-axis voltage and then accomplishes flux-weakening control without a *q*-axis current regulator. A constant *q*-axis voltage is selected with a trade-off between the maximum torque capability and efficiency of the PMSM [19]. In order to guarantee the torque capability and efficiency simultaneously, the *q*-axis voltage should be changed on the basis of the motor working state. The modified method is named current cross-coupling regulation with variable *q*-axis voltage (CCR-VQV) and its simplified diagram is shown in Fig. 1. The *q*-axis voltage is calculated from *q*-axis current and voltage limit in [20], which need optimized coefficients and remain margin to further improve the efficiency. The *q*-axis voltage is obtained by a lookup table in [21], that requires a lengthy commissioning of the motor. More critical for this paper, the methods in [19-21] cannot keep the stator voltage vector amplitude constant, then, cannot keep the inverter output voltage modulation ratio constant. Consequently, these methods cannot achieve six-step operations, although only one degree of freedom is used.

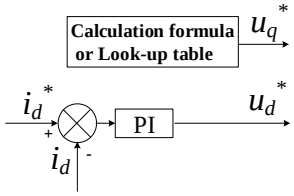

Fig. 1. *Diagram of CCR-VQV flux-weakening control*

A previous study in [22] proposes a CCR-VQV control scheme which calculates q-axis voltage from the d-axis voltage guaranteeing constant stator voltage vector amplitude. However, the method in [22] is verified in the asynchronous SVPWM linear region and without control parameter design, where the inverter switching frequency is 20 kHz. This method will be extended in this paper for high power traction motors with a maximum switching frequency in the full-speed region of 960Hz, and six-step operations are achieved to fully unitize the DC-link voltage.

The six-steps realization in [11-18] does not consider the inverter switching frequency limit. With limited switching frequency, railway traction inverters usually adopt multi-modes PWM, including asynchronous modulation, synchronous modulation and six-step single pulse modulation [23]. Asynchronous SVPWM is widely used for low-frequencies, while the six-step operation is an extension of synchronous modulation. Synchronous modulation schemes include special modulation as the selective harmonic elimination-pulse width modulation (SHEPWM) [24], and carrier based modulation as the synchronous SVPWM [25-27]. SHEPWM is widely used for traction, although the switching angle calculation needs the solution of the transcendental equation that cannot be done in real time. And there is also the problem of smooth switching to the other modes [23]. SVPWM is easy to implement digitally and the overall harmonic characteristics of some types of synchronous SVPWM are not inferior to SHEPWM [28] and therefore has been adopted in this paper for application to traction inverters.

In recent years, the focuses of PMSM flux-weakening control method study are voltage feedback current control schemes [13, 29-32] , voltage phase angle control schemes [3] and single current regulator control schemes [22]. The voltage feedback current control schemes apply double current regulators. However, these schemes are too complicated. The voltage phase angle control schemes without current regulators achieve worse current performance.

Thus, this paper explores the application of CCR-VQV in railway traction based on authors' previous study in [22], so as to achieve six-step operation with low switching frequency. Compared with the existing methods, CCR-VQV can maximize the utilization of DC voltage and achieve better dynamic performance. The method is very simple since only one current regulator is applied to achieve six-step operation. Besides, the design method of the single current regulator is given, which makes the application of the method simpler and more convenient. The structure of this paper is the following. Section II introduces the formulation of CCR-VQV flux-weakening control strategy for six-step operations. Section III illustrates the setting approach of CCR-VQV flux-weakening controller parameters and analyzes the methodology for the design of the parameters. Section IV presents the experimental tests on a 7.5 kW motor drive to validate the current control scheme proposed in this paper.

2. Single Current Regulator Control In Six-step Operations

2.1. Control Principle

In the synchronous reference frame, the steady-state voltage of interior PMSM can be expressed as (1).

$$\begin{cases} u_d = R_s i_d - \omega_r L_q i_q \\ u_q = R_s i_q + \omega_r (L_d i_d + \psi_f) \end{cases} \quad (1)$$

where u_d and u_q are the *d*-axis and *q*-axis stator voltage components; i_d and i_q are *d*-axis and *q*-axis stator current components; R_s is stator resistance; ω_r is motor electric angular speed; ψ_f is permanent magnet flux linkage; L_d and L_q are motor *d*-axis and *q*-axis inductances.

The *q*-axis current can be derived from (1) and it is equal to:

$$i_q = -\frac{\omega_r L_d}{R_s} i_d + \frac{u_q - \omega_r \psi_f}{R_s} \quad (2)$$

Equation (2) shows that, at a constant non-zero speed and *q*-axis voltage, the *d*-axis and *q*-axis steady-state current components have a linear relationship. The coupling coefficient, $-\omega_r L_d / R_s$, increases with the motor speed. When the motor speed is low, the flux-weakening control is not necessary. In fact, the maximum output voltage of the inverter is significantly higher than the back electromotive force of PMSM and the *q*-axis voltage u_q in (2) can be adjusted easily to compensate for the coupling effect with the *d*-axis current. Thus, instantaneous current control can be achieved with a double current regulators control scheme. When the motor speed increases the adjustable range of the motor voltage magnitude is reduced. The coupling effect becomes evident and the control performance of conventional double current regulators control schemes deteriorates.

Rather than eliminating the coupling effect when the motor speed is high and the voltage reaches the maximum value, single current regulator control utilizes the coupling effect to achieve flux-weakening only by regulating the *d*-axis current component. The determination of u_q in (2), in other words, the determination of *q*-axis voltage reference u_q^*

is one of the most significant procedures in the control design. It will determine the feasibility and effectivity of the algorithm.

The control of the inverter output voltage modulation ratio can be achieved by limiting the compositional stator voltage vector amplitude u_s. If the coordinate transformation maintain the vector amplitude, u_s will be equal to the motor phase voltage amplitude. If instead the power is the same, u_s will be $\sqrt{3/2}$ times the motor phase voltage amplitude. The coordinate transformation maintaining voltage vector amplitude is used in this paper and controlling u_s is equivalent to control inverter output fundamental voltage amplitude. Thus, the output voltage modulation ratio of the inverter can be controlled accurately. For the single current regulator control in this paper, the *q*-axis voltage reference u_q^* is calculated from the *d*-axis voltage reference u_d^* and target voltage vector amplitude u_s^* as:

$$u_q^* = \sqrt{u_s^{*2} - u_d^{*2}} \quad (3)$$

From (3), the current control structure of modified CCR-VQV is shown in Fig. 2.

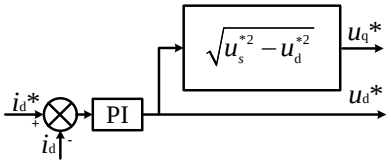

Fig. 2. *Modified CCR-VQV flux-weakening control*

In six-step operations, the amplitude of the fundamental component of output phase voltage reaches the maximum value of $2u_c/\pi$, where u_c is the inverter DC-link voltage. To operate as six-step, the target voltage vector amplitude u_s^* must also be set to $2u_c/\pi$ if the vector amplitude is kept constant in coordinate transformation. If the power is kept constant instead, u_s^* must be set to $\sqrt{6}u_c/\pi$. The instantaneous sampled and updated u_c is used to calculate u_s^* and generate the PWM pulses. Thus, the impact of u_c fluctuation on the six-step operations is eliminated. In this paper, the coordinate transformation keep the vector amplitude constant and, hence, the structure of the single current regulator for six-step operations is shown in Fig. 3.

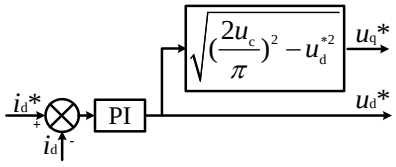

Fig. 3. *Single current regulator control in six-step operation*

In railway traction drive systems, the reference i_d^* is generated by a torque outer loop. In practical applications, the torque regulator can be replaced by a look-up table between the torque and d axis current.

2.2. Transition to Six-step Operations

Fig. 4 shows on the $i_d - i_q$ plane, the Maximum Torque Per Ampere (MTPA) curve 'OA', flux-weakening region 'AB' and 'BC' are three maximum torque working zones of PMSM at different speeds [33, 34].

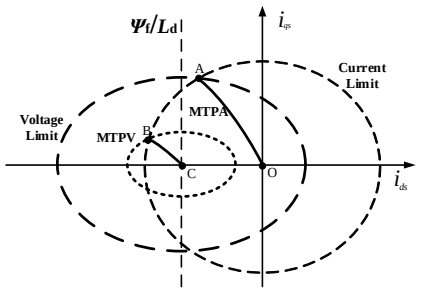

Fig. 4. *Working areas of PMSM*

The MTPA control is usually employed below the base speed and it is a typical double current regulators control. The proposed CCR-VQV single current regulator flux-weakening control is used in six-step operations. Thus, a smooth switching from MTPA and six-step operations is required.

Under the MTPA control, the reference u_s^* is lower than the maximum amplitude $2u_c/\pi$. The rule to switch from MTPA to CCR-VQV in six-step operation is:

$$\sqrt{u_q^{*2} + u_d^{*2}} \geq 2u_c/\pi \quad (4)$$

After switching to CCR-VQV in six-step operation, u_s^* is limited to $2u_c/\pi$. Thus, the voltage reference cannot be used to quit six-step operations and return to MTPA. As shown in Fig. 4, the motor operating region is divided by the MTPA curve, where six-step operation region is on the left. When the motor speed or the load reduces, the motor operation point moves to the right side of MTPA curve and should quit the six-step operation. Thus, the criteria of quitting six-step operation can be obtained by relation between the *d-q* axis current. The MTPA curve can be assumed as a straight line when switching the flux-weakening control. The criteria of switching modified CCR-VQV to MTPA is shown in (5). For non-salient pole PMSM, k=0; for salient pole PMSM, k<0.

$$i_d > ki_q, \qquad k \leq 0 \quad (5)$$

Fig. 5 describes the algorithm structure of current regulators realization. If MTPA is the current state, the flux weakening flag is equal to 0. In the step 'calculation of u_s for updating the flux weakening flag', if (4) is satisfied, the flux weakening flag will become 1. Similarly, when (5) is satisfied in six-step operation, flux weakening flag will change from 1 to 0.

Another aspect to achieve smooth switching is the necessity to avoid steps of *d-q* axis voltage reference. Tracking the current integrators is a feasible approach. When switching to six-step operation, the value of i_d current integrator in MTPA is given to i_d current integrator in modified CCR-VQV as an initialisation reset. When quitting six-step operation, the value of i_d current integrator in modified CCR-VQV is given to i_d current integrator in MTPA as an initialisation reset. At the same time, u_q^* is given to i_q current integrator in MTPA as an initialisation reset.

When other double current regulators control is used in non-flux-weakening operation, the principle of entering and quitting six-step operation is similar. But the quit criteria in (5) should be modified simply according to the specific double current regulators scheme. Take $i_d = 0$ control for example, the quit criteria is changed to be $i_d > 0$.

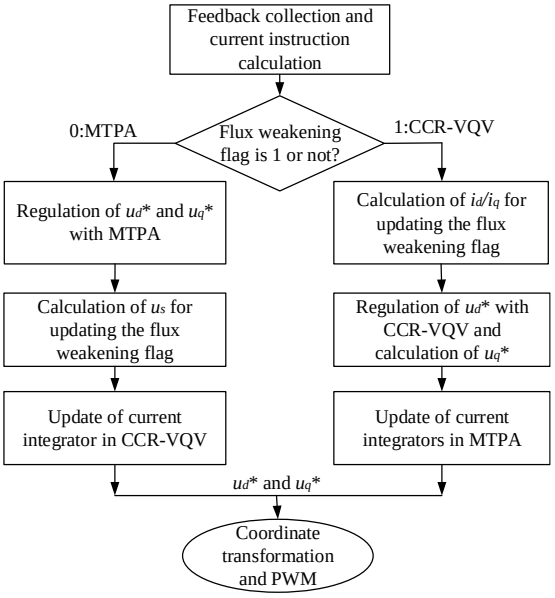

Fig. 5. *Flow chart of current regulators realization*

3. Design of The Current Regulator

3.1. Model Simplification

In practical applications it is possible to assume that the control delay T_d is $1.5T_{PWM}$, where the T_{PWM} is the control period. Therefore the modulation can be modelled by a first order transfer function with time constant T_d. The control block diagram of the proposed CCR-VQV is shown in Fig. 6, where k_p is current regulator proportional coefficient, and T_s is integral time constant.

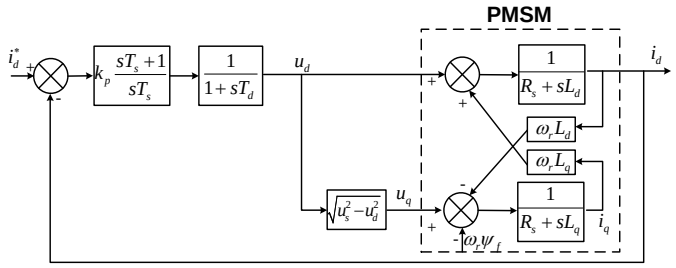

Fig. 6. *Block diagram of the proposed CCR-VQV for six-steps operations*

For the design of the control parameters of traditional double current regulators control, the back EMF can be considered as a disturbance input and assumed to be zero. Unlike the traditional schemes where the design of the two current regulators are independent, in the proposed control scheme the coupling effect between i_d and i_q cannot be ignored. So, (2) is used to calculate i_q and, then, the back EMF $\omega_r L_q i_q$. The voltage component u_q is used in (2), and according to (3) is:

$$u_q = \sqrt{u_s^2 - u_d^2} \quad (6)$$

Equation (6) should be linearized to simplify the practical implementation. The differentiation of the q-axis voltage can be expressed as:

$$\Delta u_q = -\frac{u_{d0}}{u_{q0}}\Delta u_d = k_u \Delta u_d \quad (7)$$

Where u_{d0} and u_{q0} are the steady state d-axis and q-axis voltage components, respectively. Meanwhile, using (7) u_q can be expressed as:

$$u_q = u_{q0} + \Delta u_q \quad (8)$$

Combining (8) with and (6) and (7), u_q can be obtained as:

$$u_q = \frac{u_s^2}{u_{q0}} + k_u u_d \quad (9)$$

Using (2) and (9), Fig. 6 is changed into the diagram shown in Fig. 7:

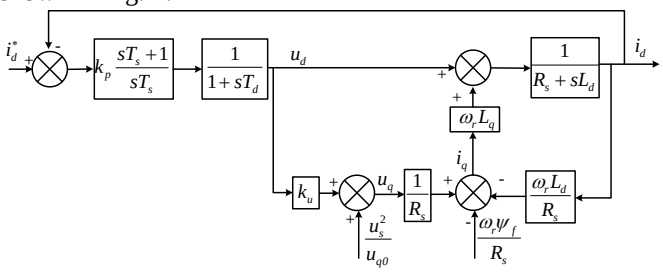

Fig. 7. *Converted control block diagram*

As u_s is a constant equal to $2u_c/\pi$ for six step operations, u_{d0}, u_{q0}, k_u and ω_r are known parameters, u_s^2/u_{q0} and $\omega_r\psi_f/R_s$ in Fig. 7 can be considered as disturbances and can be assumed to be zero for the design of the flux-weakening d-axis current regulator. Thus, based on Fig. 7, the transfer function $i_d(s)/u_d(s)$ can be expressed as:

$$\frac{i_d(s)}{u_d(s)} = \frac{1 + \frac{k_u \omega_r L_q}{R_s}}{\frac{\omega_r^2 L_q L_d}{R_s} + R_s + sL_d} \quad (10)$$

Introducing the quantities:

$$k_1 = \frac{k_u \omega_r L_q}{R_s}$$

$$k_2 = \frac{\omega_r^2 L_q L_d}{R_s}$$

$$R_s' = \frac{R_s + k_2}{1 + k_1}$$

$$L_d' = \frac{L_d}{1 + k_1}$$

equation (10) can be simplified as:

$$\frac{i_d(s)}{u_d(s)} = \frac{1}{R_s' + sL_s'} \quad (11)$$

Based on Fig. 7 and (11), the control block diagram can be simplified as shown in Fig. 8.

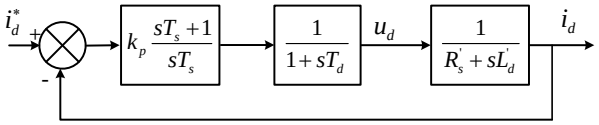

Fig. 8. *Simplified control block diagram*

3.2. Design of The Regulator Parameters

The simplified control block diagram in Fig. 8 is a classical second order system, for which the pole-zero cancellation method can be used to design the controller parameters. As an inner current control loop, response speed in millisecond range is set as design goal. [35, 36]

The forward transfer function G_{OL} for the above block diagram can be expressed as:

$$G_{OL} = \frac{k_p}{T_s R_s'} \frac{(sT_s + 1)}{s} \frac{1}{(1 + sT_d)} \frac{1}{(1 + sT_\sigma')} \quad (12)$$

where,

$$T_\sigma' = \frac{L_s'}{R_s'} = \frac{R_s L_d}{R_s^2 + \omega_r^2 L_q L_d} \quad (13)$$

It should be noted that for flux-weakening operations ω_r is very large, and then T_σ' is very small. Using the parameters given in TABLE I, which refer to the experimental PMSM used in this paper, T_σ' would be $2 \times 10^{-4} s$ for a motor speed $n = 1200 rpm$. Meanwhile assuming a maximum switching frequency of 1 kHz that is typical of traction inverters, the delay $T_d = 1.5 T_{PWM} > 1.5 \times 10^{-3}$ and, hence, $T_d \gg T_\sigma'$. In the controller parameters design, the integral time constant T_s is used to eliminate the larger time constant, so:

$$T_s = T_d \quad (14)$$

Table 1 Parameters of the experimental PMSM

Parameter	Value
Rated power (kW)	7.5
Rated voltage (V)	380
q-axis inductance (mH)	100
d-axis inductance (mH)	50
PM flux linkage (Wb)	1.25
Pole pairs	2
Coil resistance (Ω)	1.3

Then, (12) can be simplified as:

$$G_{OL} = \frac{k_p}{T_d R_s'} \frac{1}{s(1 + sT_\sigma')} \quad (15)$$

In order to balance the system response speed and overshoot, the damping coefficient ξ of the closed-loop transfer function is set as $1/\sqrt{2}$. Then the following relationship is obtained:

$$\frac{k_p}{T_d R_s'} T_\sigma' = \frac{1}{2} \quad (16)$$

Thus, the final design of the flux-weakening *d*-axis current controller parameters is:

$$\begin{cases} k_p = \dfrac{T_d R_s'}{2T_\sigma'} \\ k_i = \dfrac{k_p}{T_s} = \dfrac{R_s'}{2T_\sigma'} \end{cases} \quad (17)$$

where, k_i is current regulator integral coefficient.

3.3. Result Analysis

With the control parameters in (17), the final expression of the closed-loop transfer function is

$$G_{CL} = \frac{1}{2T_\sigma'^2} \frac{1}{s^2 + \frac{1}{T_\sigma'} s + \frac{1}{2T_\sigma'^2}} \quad (18)$$

In the above design process, k_u and ω_r are relevant to PMSM operations and are taken as parameters. The physical meaning of k_u needs to be further clarified. According to literature [14-16], the voltage phase angle θ is defined as:

$$\theta = \tan^{-1}(-\frac{u_d}{u_q}) \quad (19)$$

From (7) for steady state conditions, the voltage phase angle θ is:

$$\theta = \tan^{-1}(k_u) \quad (20)$$

Then, the PMSM steady state electromagnetic torque T_e can be expressed as:

$$T_e = -\frac{3P_n}{4L_d L_q \omega_r^2} [-2 \sin(\tan^{-1}(k_u))\, \omega_r L_q \psi_f U_s - (L_d - L_q) U_s^2 \sin(2 \tan^{-1}(k_u))] \quad (21)$$

Using the motor parameters in TABLE I, the relation between T_e and k_u is shown in Fig. 9 for a mechanical speed of 1200 rpm.

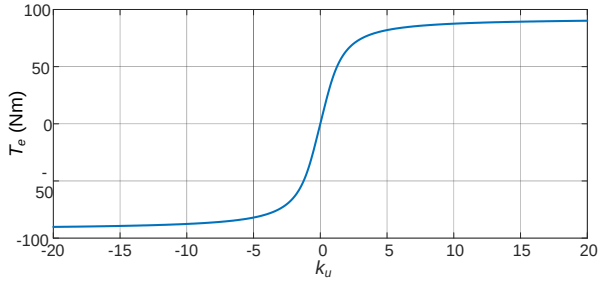

Fig. 9. *The relation between torque and k_u*

As shown in (18), T_σ' is the only parameter that influences the closed-loop transfer function. According to T_σ' expression in (13), k_u has been eliminated in (18). This means the design formulae given by (17) are not influenced by the PMSM torque.

With reference to the normalized transfer function of a second order system without zeros, the natural frequency ω_0 of (18) is:

$$\omega_0 = \frac{\sqrt{2}}{2} \frac{R_s^2 + \omega_r^2 L_q L_d}{R_s L_d} \quad (22)$$

As well-known from basic control theory, the response of the system is faster for larger ω_0. So the system response is faster if the motor speed ω_r is larger based on above design result.

Fig. 10 shows response of i_d in per unit for a step change of i_d^* for motor speeds of 1200 rpm, 1600 rpm and 2000 rpm. The response time is less than 1.5ms while overshoot is less than 5%.

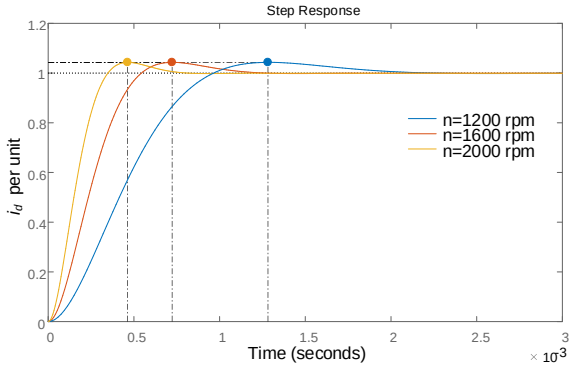

Fig. 10. *The step response of the design with different motor speed*

3.4. Stability Analysis

With the control parameters in (17), the final expression of the open-loop transfer function is

$$G_{OL} = \frac{1}{2T_\sigma'^2} \frac{1}{s^2 + \frac{1}{T_\sigma'} s} \quad (23)$$

Based on (23), the bode diagram for motor speeds of 1200rpm, 1600rpm, and 2000rpm can be obtained as Fig. 11. It can be seen that both the amplitude margin and the phase margin are positive. Consequently, the system is stable.

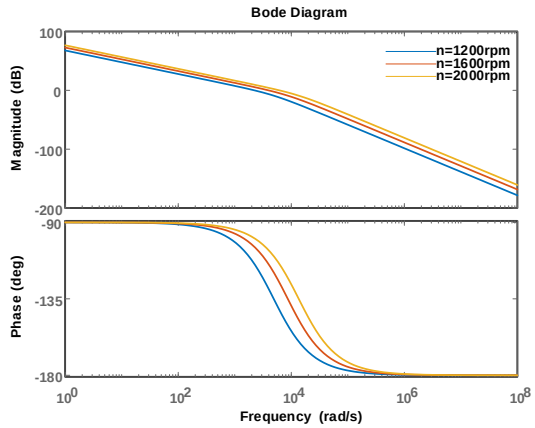

Fig. 11. *The bode diagram*

4. Experimental Verification

The rig used for the experimental verification is shown in Fig. 12 and includes a 7.5 kW PMSM motor, a two-level inverter controlled by a TMS320F28335 floating point digital signal processor. A twin motor is used as a load and allows the control of the torque. The main PMSM parameters are shown in TABLE I.

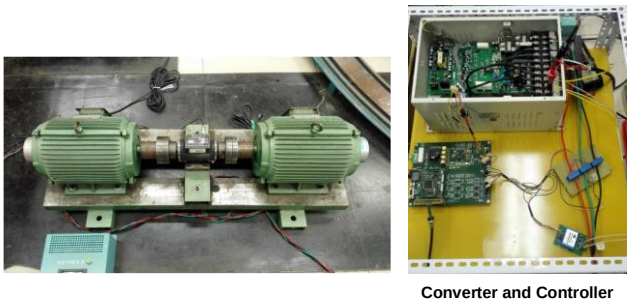

Fig. 12. *7.5kW PMSM test rig*

4.1. PWM Scheme of The Inverter

The motor has been controlled with a simplified multi-mode PWM that limits the switching frequency of the inverter. Fig. 13 shows the switching frequency f_c as a function of the fundamental frequency f_s, and m is the voltage modulation ratio. For frequencies up to 30 Hz, the asynchronous SVPWM is used with constant switching frequency at 960 Hz. For higher fundamental frequencies, a synchronous 11-pulse Basic Bus Clamping Strategy (BBCS) SVPWM is used instead [25, 26]. BBCS synchronous SVPWM ensures half-wave odd symmetry, 1/4 period even symmetry and three-phase symmetry of the output voltage, and thus optimizes the harmonic characteristics. When the fundamental frequency increases further, the BBCS SVPWM with 11 pulses enters in the overmodulation region and the pulses decrease to 7, 5 and finally enters six-step operations.

In the first test, the motor accelerates from 0 rpm with constant acceleration. Fig. 14 presents the motor phase voltage, phase current and synchronous SVPWM vector composition section. Fig. 14a shows that when the stator frequency is 30 Hz, corresponding to a speed of 900 rpm, the inverter switches from SVPWM to BBCS synchronous SVPWM. When the frequency increases further, the number of pulses decreases (Fig. 14b) until the modulation enters six-step operations (Fig. 14c). The transition between of the different modulation modes is smooth as predicted by the theoretical analysis, and the phase current symmetry is maintained.

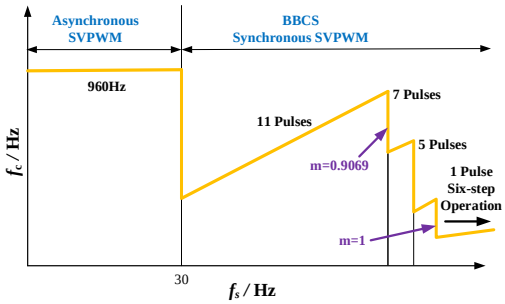

Fig. 13. *PWM scheme of the inverter*

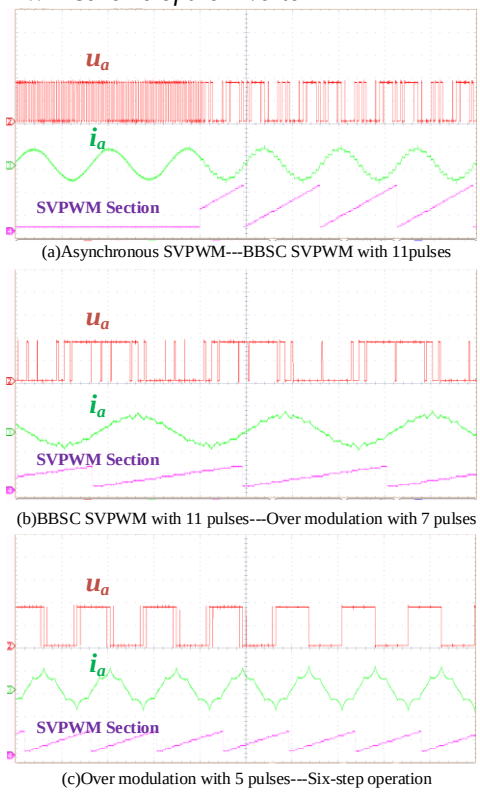

(a)Asynchronous SVPWM---BBSC SVPWM with 11pulses

(b)BBSC SVPWM with 11 pulses---Over modulation with 7 pulses

(c)Over modulation with 5 pulses---Six-step operation

Fig. 14. *PWM in full speed range*

4.2. Speed Closed-loop Test

In the second test, the motor accelerates without load from 0 rpm to 1700 rpm, remains at constant speed for 3 s and finally decelerates down to 0 rpm. Below the base speed, a double current regulators control is used, where the reference for i_d is set at -2 A and the reference for i_q is given by the speed regulator. Six-step operations start when the voltage reference is equal to the value indicated by (4), and the proposed CCR-VQV is used.

Fig. 15 presents the measurements of n, i_d, i_q, u_s and u_d. The region between the two blue vertical lines is when the inverter operates in six-steps. The acceleration and deceleration is not affected by the transition and there is also no obvious spike or oscillation on the speed, current and voltage diagrams. When the inverter enters in six-step operations, i_d decreases when the speed increases and vice-

versa to regulate the flux linkage. The voltage u_s is constant and equal to be maximum value $2u_c/\pi$ in conformity with the theoretical expectations.

Fig. 16(a) shows the waveforms of the line voltage and phase current when the inverter enters six-step operations. Fig. 16(b) shows the same waveforms for a constant motor speed equal to 1700rpm, while Fig. 16(c) shows the same waveforms when the inverter exits six-step operations. The phase current does not have any spikes during the transition between the two modes and the line voltage is firmly in six-step operations, unlike other control scheme that shows a narrow pulse at the maximum and minimum of the waveform. Thus, the designed current regulator can stably realize switching between MTPA and CCR-VQV in six-step operations without obvious spike.

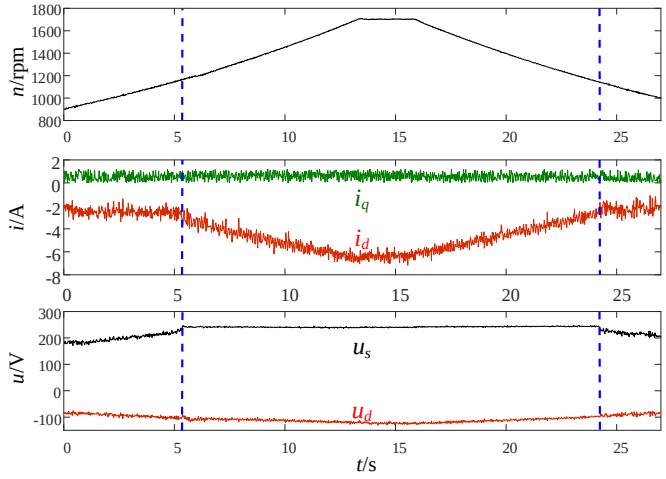

Fig. 15. *Experiment results of the closed-loop speed control*

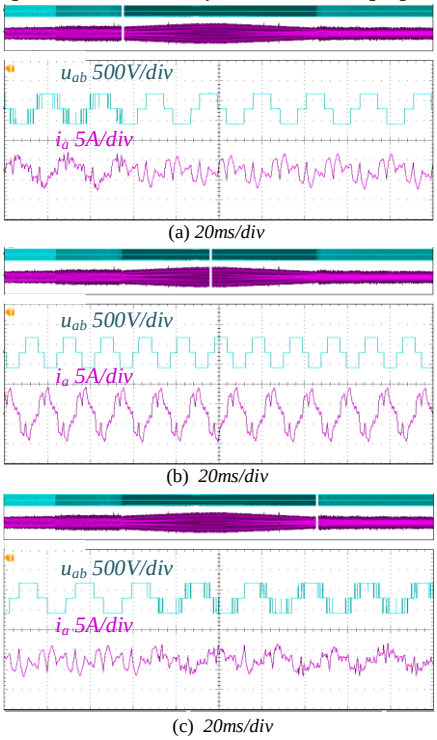

Fig. 16. *Line voltage and phase current of speed closed-loop control*

The experimental results of Fig. 15 and Fig. 16 can prove that CCR-VQV can be applied to railway traction, because the method can achieve not only low switching frequency, but also full-speed range operation, especially six-step operation.

4.3. Six-step Operation Current Stepping Test

In the third test, the machine speed is constant at 1200 rpm. The inverter operates in six-steps with the proposed CCR-VQV. The d-axis current reference is changed as a step from -2 A to -4.5 A at 1.5 s, from -4.5 A to -7 A at 4 s, from -7 A to -4.5 A at 6.5 s, and finally from -4.5 A to -2 A at 9 s. Fig. 17 shows the waveform of i_d^*, i_d and i_q. i_d follows the reference i_d^* rapidly at all the stepping point. i_q changes with i_d, which consists with the theory. It can be obviously seen that the designed current regulator has achieved excellent dynamic tracking performance and stability performance.

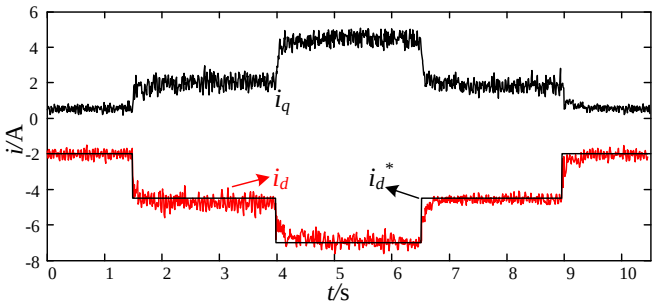

Fig. 17. *Step response in six-step operation*

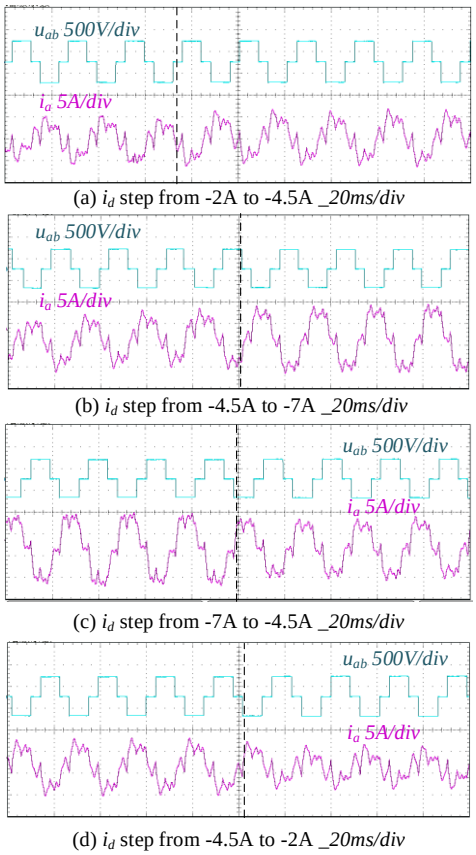

Fig. 18. *Line voltage and phase current of current step response in six-step operation*

Fig. 18 shows the waveforms of motor line voltage and phase current around the stepping times of the *d*-axis current. The inverter is always in six-step operations and the motor phase current response is in agreement with the design values in millisecond range. This confirms that the single current regulator scheme ensures a good dynamic of the PMSM for flux-weakening control in six-step operations. Based on the experimental results of Fig. 17 and Fig. 18, it

can be found that the designed current controller is superior in current tracking and dynamic response, which can achieve satisfactory six-step operation.

5. Conclusion

This paper proposes a novel current closed-loop control scheme for six-step operations of traction PMSMs. Considering that in this region the magnitude of the voltage is constant and the only degree of freedom is the phase angle, the proposed control uses a single current regulator to achieve instantaneous motor current control. The paper has then proposed a reliable strategy to switch from the double current regulators control to the single current regulator control and it has demonstrated that there are no current spikes during the transition between the two schemes. The design of the controller parameters has been analyzed to understand the main quantities affecting the dynamic of the motor when controlled by a single current regulator. Experimental results on a 7.5 kW PMSM with a maximum switching frequency of 960 Hz have confirmed all the theoretical hypotheses. Compared with conventional methods, the proposed solution is simple and easy to implement and is not affected by the accuracy of motor parameters

6. Acknowledgments

This paper and its related research are supported by grants from the Power Electronics Science and Education Development Program of Delta Group (DREG2019017) and the Fundamental Research Funds for the Central Universities (2019JBM061).

7. References

[1] K. Kondou and K. Matsuoka, 'Permanent magnet synchronous motor control system for railway vehicle traction and its advantages', Proc. Int. Power Conversion Conference - Nagaoka 1997., vol.1, pp. 63-68.
[2] I. Spina, A. D. Pizzo, L. Beneduce, B. Cascone, and L. Fratelli, 'Comparative analysis of performance and energy losses in light railways vehicles equipped with IM or PMSM drive', Proc. Int. International Symposium on Power Electronics, Electrical Drives, Automation and Motion, 2014, pp. 566-572.
[3] X. Fang, T. Wang, Z. Yang, and F. Lin, 'Permanent magnet synchronous traction motor torque close-loop control based on stator flux observation for urban rail train', Proc. Int. Asian Conference on Energy, Power and Transportation Electrification (ACEPT), 2016, pp. 1-6.
[4] S. Morimoto, M. Sanada, and Y. Takeda, 'Wide-speed operation of interior permanent magnet synchronous motors with high-performance current regulator', IEEE Transactions on Industry Applications, 1994.,vol. 30, no. 4, pp. 920-926.
[5] P. Ching-Tsai and S. M. Sue, 'A linear maximum torque per ampere control for IPMSM drives over full-speed range', IEEE Transactions on Energy Conversion, 2005, vol. 20, no. 2, pp. 359-366.
[6] B. Bon-Ho, N. Patel, S. Schulz, and S. Seung-Ki, 'New field weakening technique for high saliency interior permanent magnet motor', Proc. Int. IAS Annual Meeting on Conference Record of the Industry Applications Conference, 2003., vol. 2, pp. 898-905.
[7] R. U. Lenke, R. W. D. Doncker, M. S. Kwak, T. S. Kwon, and S. K. Sul, 'Field weakening control of interior permanent magnet machine using improved current interpolation technique', Proc. Int. 37th IEEE Power Electronics Specialists Conference, 2006, pp. 1-5.
[8] Y. Young-Doo, L. Wook-Jin, and S. Seung-Ki, 'New flux weakening control for high saliency interior permanent magnet synchronous machine without any tables', Proc. Int. European Conference on Power Electronics and Applications, 2007, pp. 1-7.
[9] K. Jang-Mok and S. Seung-Ki, 'Speed control of interior permanent magnet synchronous motor drive for the flux weakening operation', IEEE Transactions on Industry Applications, 1997, vol. 33, no. 1, pp. 43-48.
[10] P. Ching-Tsai and L. Jenn-Horng, 'A robust field-weakening control strategy for surface-mounted permanent-magnet motor drives', IEEE Transactions on Energy Conversion, 2005, vol. 20, no. 4, pp. 701-709.
[11] T. S. Kwon, G. Y. Choi, M. S. Kwak, and S. K. Sul, 'Novel Flux-Weakening Control of an IPMSM for Quasi-Six-Step Operation', IEEE Transactions on Industry Applications, 2008, vol. 44, no. 6, pp. 1722-1731.
[12] Y. C. Kwon, S. Kim, and S. K. Sul, 'Voltage Feedback Current Control Scheme for Improved Transient Performance of Permanent Magnet Synchronous Machine Drives', IEEE Transactions on Industrial Electronics, 2012,vol. 59, no. 9, pp. 3373-3382.
[13] Y. C. Kwon, S. Kim, and S. K. Sul, 'Six-Step Operation of PMSM With Instantaneous Current Control', IEEE Transactions on Industry Applications, 2014, vol. 50, no. 4, pp. 2614-2625.
[14] B. K. Bose, 'A high-performance inverter-fed drive system of an interior permanent magnet synchronous machine', IEEE Transactions on Industry Applications, 1988, vol. 24, no. 6, pp. 987-997.
[15] T. Schoenen, A. Krings, D. v. Treek, and R. W. D. Doncker, 'Maximum DC-link voltage utilization for optimal operation of IPMSM', IEEE, International Electric Machines and Drives Conference, 2009, pp. 1547-1550.
[16] T. Miyajima, H. Fujimoto, and M. Fujitsuna, 'A Precise Model-Based Design of Voltage Phase Controller for IPMSM', IEEE Transactions on Power Electronics, 2013, vol. 28, no. 12, pp. 5655-5664.
[17] S. Kim and J. K. Seok, 'Maximum Voltage Utilization of IPMSMs Using Modulating Voltage Scalability for Automotive Applications', IEEE Transactions on Power Electronics, 2013, vol. 28, no. 12, pp. 5639-5646.
[18] J. Park, S. Jung, and J. I. Ha, 'Variable Time Step Control for Six-Step Operation in Surface-Mounted Permanent Magnet Machine Drives', IEEE Transactions on Power Electronics, 2018, vol. 33, no. 2, pp. 1501-1513.
[19] S. Chi and L. Xu, 'A special flux-weakening control scheme of pmsm - incorporating and adaptive to wide-range speed regulation', CES/IEEE, 5th International Power Electronics and Motion Control Conference, 2006, vol. 2, pp. 1-6.
[20] S. Chi, L. Xu, and Z. Zhang, 'Efficiency-Optimized Flux-Weakening Control of PMSM Incorporating Speed Regulation', IEEE, Power Electronics Specialists Conference, 2007, pp. 1627-1633.
[21] Y. Zhang, L. Xu, M. K. Guven, S. Chi, and M. S. Illindala, 'Experimental verification of deep flux-weakening operation of a 50 kW IPM machine by using single current regulator', IEEE, Energy Conversion Congress and Exposition, 2009, pp. 3647-3652.

[22] F. Xiaochun, L. Fei, and Y. Zhongping, 'A modified flux-weakening control method of PMSM based on the d-q current cross-coupling effect', IEEE, Conference and Expo Transportation Electrification Asia-Pacific (ITEC Asia-Pacific), 2014, pp. 1-6.
[23] X. Fang, F. Lin, and Z. Yang, 'An Improved Central 60 Synchronous Modulation for High Transient Performance with PMSM Stator Flux Control Used in Urban Rail Transit Systems', Journal of Power Electronics, 2016, vol. 16, no. 2, pp. 542-552.
[24] S. R. Bowes and D. Holliday, 'Optimal Regular-Sampled PWM Inverter Control Techniques', IEEE Transactions on Industrial Electronics, 2007, vol. 54, no. 3, pp. 1547-1559.
[25] G. Narayanan and V. T. Ranganathan, 'Synchronised PWM strategies based on space vector approach. I. Principles of waveform generation', IEE Proceedings - Electric Power Applications, 1999, vol. 146, no. 3, pp. 267-275.
[26] G. Narayanan and V. T. Ranganathan, 'Two novel synchronized bus-clamping PWM strategies based on space vector approach for high power drives', IEEE Transactions on Power Electronics, vol. 17, no. 1, pp. 84-93, 2002.
[27] C. Wang, K. Wang, and X. You, 'Research on Synchronized SVPWM Strategies Under Low Switching Frequency for Six-Phase VSI-Fed Asymmetrical Dual Stator Induction Machine', IEEE Transactions on Industrial Electronics, 2016, vol. 63, no. 11, pp. 6767-6776.
[28] W. Kun, Y. Xiaojie, W. Chenchen, and Z. Minglei, 'Research on the comparison of synchronized modulation of SHEPWM and SVPWM under low switching frequency', Transactions of China Electrotechnical Society, 2015, vol. 30, no. 14, pp. 333-341.
[29]Chao Wang and Z. Q. Zhu, 'Fuzzy Logic Speed Control of Permanent Magnet Synchronous Machine and Feedback Voltage Ripple Reduction in Flux-Weakening Operation Region', IEEE Transactions on Industry Applications, April 2020, vol. 56, no. 2, pp. 1505 – 1517.
[30] Wei Xu ; Moustafa Magdi Ismail ; Yi Liu ; Md Rabiul Islam, 'Parameter Optimization of Adaptive Flux-Weakening Strategy for Permanent-Magnet Synchronous Motor Drives Based on Particle Swarm Algorithm', IEEE Transactions on Power Electronics, April 2019, pp. 12128-12140.
[31] L´eopold Sepulchre, Maurice Fadel, Maria Pietrzak-David, Member, 'MTPV Flux-Weakening Strategy for PMSM High Speed Drive', IEEE Transactions on Industry Applications, Dec 2018, vol. 54, no. 6, pp. 6081 – 6089.
[32] Hesong Liu, Z. Q. Zhu, Essam Mohamed, Yongling Fu, and Xiaoye Qi, 'Flux-Weakening Control of Nonsalient Pole PMSM Having Large Winding Inductance, Accounting for Resistive Voltage Drop and Inverter Nonlinearities', IEEE Transactions on Power Electronics, February 2012, vol. 27, no. 2, pp. 942-952.
[33] T. M. Jahns, G. B. Kliman, and T. W. Neumann, 'Interior Permanent-Magnet Synchronous Motors for Adjustable-Speed Drives', IEEE Transactions on Industry Applications, 1986, vol. IA-22, no. 4, pp. 738-747.
[34] S. Morimoto, Y. Takeda, T. Hirasa, and K. Taniguchi, 'Expansion of operating limits for permanent magnet motor by current vector control considering inverter capacity', IEEE Transactions on Industry Applications, 1990, vol. 26, no. 5, pp. 866-871.
[35] W. Leonhard, 'Control of electrical drives',. Springer Science & Business Media, 2012.
[36] S. K. Sahoo and T. Bhattacharya, 'Field Weakening Strategy for a Vector-Controlled Induction Motor Drive Near the Six-Step Mode of Operation', IEEE Transactions on Power Electronics, 2016, vol. 31, no. 4, pp. 3043-3051.